Guide-Wire Tracking During Endovascular Interventions

Shirley A. M. Baert*, Max A. Viergever, *Member, IEEE*, and Wiro J. Niessen, *Member, IEEE*

***Abstract*—A method is presented to extract and track the position of a guide wire during endovascular interventions under X-ray fluoroscopy. The method can be used to improve guide-wire visualization in low-quality fluoroscopic images and to estimate the position of the guide wire in world coordinates. A two-step procedure is utilized to track the guide wire in subsequent frames. First, a rough estimate of the displacement is obtained using a template-matching procedure. Subsequently, the position of the guide wire is determined by fitting a spline to a feature image. The feature images that have been considered enhance line-like structures on: 1) the original images; 2) subtraction images; and 3) preprocessed images in which coherent structures are enhanced. In the optimization step, the influence of the scale at which the feature is calculated and the additional value of using directional information is investigated. The method is evaluated on 267 frames from ten clinical image sequences. Using the automatic method, the guide wire could be tracked in 96% of the frames, with a similar accuracy to three observers, although the position of the tip was estimated less accurately.**

***Index Terms*—Guide-wire tracking, image enhancement, interventional radiology, splines.**

I. Introduction

ENDOVASCULAR interventions are rapidly advancing as an alternative for invasive classical vascular surgery. During these interventions, a guide wire is inserted into the groin and is advanced under fluoroscopic guidance. Accurate positioning of the guide wire with respect to the vasculature is a prerequisite for a successful procedure. Especially during neuro-interventions, positioning the guide wire correctly is difficult because of the complexity of the vasculature and narrowness of the blood vessels, which causes an increase in intervention time and radiation exposure.

Owing to the low dose used in fluoroscopy in order to minimize the radiation exposure of the patient and radiologist, image quality is often limited. Motion artefacts, due to patient motion or device motion, also introduce limitations to image quality.

In this paper, a method to track the position of the guide wire is presented, which can deal with the low signal-to-noise ratio (SNR) inherent to fluoroscopic images. The method has the following two main purposes.

- In a calibrated C-arm system, the position of the guide wire in fluoroscopy images can be used to estimate its position in three dimensions. It is then possible to use the method as a navigation tool in interventional radiology, e.g., by displaying the guide wire in three-dimensional (3-D) images (3DRX, MRA), obtained prior to the intervention.
- A possible reduction in radiation exposure can be achieved by enhancing the guide-wire visualization in low-dose fluoroscopy images.

The motivation of this paper is mainly to serve as a preprocessing step for navigation purposes.

There is relatively little literature on tracking guide wires from two-dimensional (2-D) fluoroscopy images. In [1], the possibility to use guide-wire identification to extract information regarding myocardial function is evaluated. However, the guide wire was only extracted in a single frame and not in time. Other research has been directed toward active tracking of guide wires and catheters to control their position inside the human body using external devices [2], [3] or to reconstruct 3-D catheter paths [4].

There has been a considerable amount of work on the enhancement and extraction of curved line structures. In medical imaging, it is used to extract anatomical features such as (centerlines of) blood vessels, e.g., [5]–[14]. In remote sensing, it is applied to extract roads, rivers, and valleys from satellite images or low-resolution aerial imagery, e.g., [15] and [16].

An extensive work on tracking contours can be found in computer vision, e.g., in feature extraction from faces [17], [18] or moving objects [19].

Compared with previous work, our method focuses on tracking of guide wires in a sequence of images rather than extracting the guide wire in a single frame. Also, in our approach, we evaluate several techniques for line enhancement, prior to estimating the position of the guide wire. Lastly, a thorough accuracy analysis of the method has been performed with manual tracings as reference standard. This gives a clear indication of algorithm accuracy for, e.g., applications as navigation.

This paper is organized as follows. In Section II, the tracking procedure is presented, which is based on the energy minimization of a B-spline parameterization of the guide wire in a feature image. The feature image is constructed by enhancing line-like structures of the correct orientation, with or without subtraction or coherence enhancing diffusion (CED) as a preprocessing step. In Section III, the evaluation protocol to determine the accuracy of the algorithm with respect to a reference standard provided by two trackings of three observers is discussed. Section IV presents the results of the evaluation for

Manuscript received July 23, 2002; revised February 24, 2003. The Associate Editor responsible for coordinating the review of this paper and recommending its publication was D. Hawkes. *Asterisk indicates corresponding author.*

*S. A. M. Baert is with the Image Sciences Institute, University Medical Center Utrecht, Heidelberglaan 100, Room E.01.334, 3584 CX Utrecht, The Netherlands (e-mail: shirley@isi.uu.nl).

M. A. Viergever and W. J. Niessen are with the Image Sciences Institute, University Medical Center Utrecht, 3584 CX Utrecht, The Netherlands (e-mail: max@isi.uu.nl; wiro@isi.uu.nl).

Digital Object Identifier 10.1109/TMI.2003.815904

the different types of feature images that have been considered. Section V concludes with a discussion and suggestions for further research.

II. Methods

In order to represent the guide wire, a spline parameterization is used. For all experiments in this paper, we used a third-order B-spline curve defined by

$$\mathbf{C}(u) = \sum_{i=0}^{p} N_{i,3}(u)\mathbf{P}_i, \qquad 0 \le u \le 1 \tag{1}$$

where $\mathbf{P}_i$ denote the control points (forming a control polygon), $p+1$ is the number of control points, and $N_{i,3}(u)$ is the third-degree B-spline basis functions defined on the nonperiodic knot vector

$$U = \{0, \ldots, 0, u_4, \ldots, u_{m-4}, 1, \ldots, 1\} \tag{2}$$

where m is the number of knots.

In order to find the spline in frame $n+1$ if the position in frame n is known, a two-step procedure is introduced. First, a rigid translation is determined to capture the rough displacement of the spline. Next, a spline optimization procedure is performed in which the spline is allowed to deform for accurate localization of the guide wire. These steps can be understood as a coarse-to-fine strategy, where the first step ensures a sufficiently good initialization for the spline optimization. Since we focused on the tracking of the guide wire, initialization in the first frame is currently achieved using manual outlining.

A. Rigid Transformation

In order to obtain a first estimate of the displacement, a binary template is constructed based on the position in the present frame. This template is set equal to the size of the spline in the present frame. The best location of this template in the new frame can be obtained by determining the highest cross correlation of the frame with a certain search region in this image (or features derived from it; see Section II-C3). The size of this search region is defined as three times the width and three times the height of the template.

The template matching technique is based on the assumption that a local displacement, i.e., $\mathbf{d} = (d_x, d_y)$, of a structure in one image I_0 can be estimated by defining a certain window W (say, $K \times L$ pixels in size) containing this structure, and by finding the corresponding window in a second image I in the sequence by means of correlation. The correlation coefficient (CC) is computed as

$$\mathrm{CC}(\mathbf{d}) = \frac{\sum_{\mathbf{x}\in W}[I_0(\mathbf{x}) - \langle I_0\rangle][I(\mathbf{x}+\mathbf{d}) - \langle I\rangle_{\mathbf{d}}]}{\sqrt{\sum_{\mathbf{x}\in W}[I_0(\mathbf{x}) - \langle I_0\rangle]^2 \sum_{\mathbf{x}\in W}[I(\mathbf{x}+\mathbf{d}) - \langle I\rangle_{\mathbf{d}}]^2}} \tag{3}$$

where

$$\langle I_0\rangle = \frac{1}{KL}\sum_{\mathbf{x}\in W} I_0(\mathbf{x}) \tag{4}$$

and

$$\langle I\rangle_{\mathbf{d}} = \frac{1}{KL}\sum_{\mathbf{x}\in W} I(\mathbf{x}+\mathbf{d}) \tag{5}$$

denote the mean values of the image intensities in the respective windows.

B. Spline Optimization

After performing the rigid translation, the spline is optimized under internal and external forces. The internal constraints are related to the geometry of the curve and influence the length (first derivative of the B-spline) and the curvedness (second derivative of the spline). This curvature (κ) is computed as

$$\kappa = \int_0^1 \frac{|\mathbf{C}'(s) \times \mathbf{C}''(s)|}{l^3}\, ds \tag{6}$$

where l is the length of the curve given by

$$l = \int_0^1 \mathbf{C}'(s)\, ds \tag{7}$$

expressed in 1/mm^2. For the external forces, the image intensity or a feature image derived from it (see Section II-C3) is used. The total energy is then calculated as follows:

$$E = \alpha \sum_{i=0}^{n} \big(\mathbf{x}\kappa^2(i) + F(i)\big) \cdot l(i) \tag{8}$$

with κ denoting the curvature as calculated above, $l(i)$ denoting the length of the segment associated with sample point i, F denoting the normalized external energy, and n denoting the number of samples points, which is 100 in this case, and α denoting a constant, which is chosen as 6.25 in all experiments. The spline contains four or five control points. The spline is optimized using Powell's direction set method [20].

C. External Image Force

Using original images for the matching and optimization steps, the guide wire cannot effectively be tracked due to presence of other objects in the image and/or due to the low SNR of the images. Therefore, a filter that enhances line-like structures of the correct orientation is considered. Also, two preprocessing techniques are considered, i.e., 1) the use of subtraction images to reduce the background (see Section II-C1) and 2) the use of nonlinear smoothing algorithms to reduce noise while maintaining line-like structures (see Section II-C2).

1) Subtraction Image: To remove disturbing structures such as stitches or ribs in the neighborhood of the guide wire, subtraction images can be constructed. These images are obtained by subtracting the first frame from frame n. The first frame is used to ensure sufficient guide-wire movement so as to make it clearly visible in the subtraction image. In our experiments, we used image sequences with a maximum of 49 frames. For longer sequences, the image to be subtracted can be updated, e.g., by taking the current image minus the mth image, to limit the effects of background motion. Alternatively, methods for motion correction in subtraction techniques can be used [21].

2) Coherence-Enhancing Diffusion: To reduce the noise in the fluoroscopic images, a nonlinear diffusion technique is included, in which coherent flow-like textures are enhanced [22]. The diffusion equation is given by

$$\partial_t I(\mathbf{x};t) = \nabla \cdot \big(D\nabla I(\mathbf{x};t)\big). \tag{9}$$

where D denotes the conduction coefficient. In case of linear diffusion D is a constant.

Weickert [22] presents an extension of the diffusion equation by replacing the scalar-valued coefficient D by a diffusion tensor $\mathbf{D}$, which depends on the image structure. Hereto, the local first-order structure is studied by considering the structure tensor $\mathbf{M}$ as follows:

$$\mathbf{M} = \nabla I(\mathbf{x};\sigma)\nabla I(\mathbf{x};\sigma)^T \tag{10}$$

with eigenvalues μ_1 and μ_2 ($\mu_1 \geq \mu_2$) and the corresponding orthonormal eigenvectors $\mathbf{v}_1$ and $\mathbf{v}_2$. The gradient is computed using Gaussian scaled derivative operations at a scale σ [see also (17)]. Using diffusion based on the structure tensor, not only the amount, but also the direction of diffusion can be regulated. Smoothing along the coherence direction $\mathbf{v}_2$ with a diffusity λ_2, which increases with respect to the coherence $(\mu_1 - \mu_2)^2$, gives an enhancement of the coherent structures in an image. This is achieved by constructing $\mathbf{D}$ from the following system of orthonormal eigenvectors:

$$\mathbf{v}_1 \parallel \nabla I(\mathbf{x};\sigma) \tag{11}$$

$$\mathbf{v}_2 \perp \nabla I(\mathbf{x};\sigma) \tag{12}$$

and eigenvalues

$$\lambda_1 = \alpha \tag{13}$$

$$\lambda_2 = \begin{cases} \alpha, & \text{if } \mu_1 = \mu_2 \\ \alpha + (1-\alpha)\exp\left(\dfrac{-C}{(\mu_1 - \mu_2)^2}\right), & \text{else} \end{cases} \tag{14}$$

with $C \geq 0$ and $\alpha \in (0,1)$, which keeps $\mathbf{D}$ uniformly positive definite. Fig. 1 shows an example of a part of a frame preprocessed using CED.

3) Feature Image: To determine the spline position, a feature image is used in which line-like structures are enhanced. The feature image is determined from the original image and the image preprocessed with subtraction or CED.

In order to enhance elongated structures in the image, the eigenvalues of the Hessian matrix are calculated at scale σ. This Hessian matrix is defined as

$$H = \begin{pmatrix} I_{xx} & I_{xy} \\ I_{yx} & I_{yy} \end{pmatrix} \tag{15}$$

where I_{xy} represents the convolution with the scaled Gaussian derivative

$$I_{xy} = I * \frac{\partial^2}{\partial x \partial y} G(\mathbf{x},\sigma) \tag{16}$$

and $G(\mathbf{x},\sigma)$ is given as

$$G(\mathbf{x},\sigma) = \frac{1}{2\pi\sigma^2} e^{(-\mathbf{x}^2/2\sigma^2)}. \tag{17}$$

The corresponding eigenvalues are given by

$$\lambda_{1,2}(\mathbf{x},\sigma) = \frac{1}{2}\left(I_{xx} + I_{yy} \pm \sqrt{(I_{xx} - I_{yy})^2 + 4I_{xy}^2}\right). \tag{18}$$

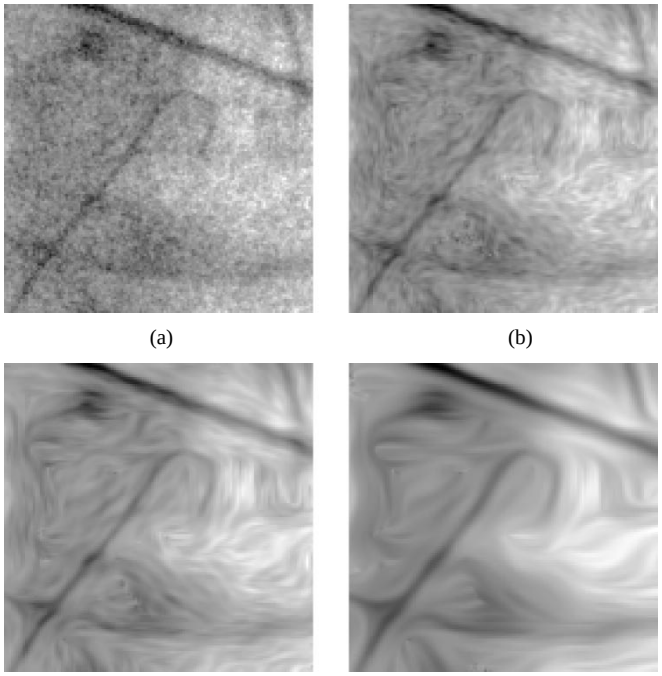

Fig. 1. Part of the original image. (a) A fluoroscopic image of a guide wire in the thorax. The same part of the image preprocessed using coherence enhancing diffusion with: (b) $t = 5$, (c) $t = 20$, and (d) $t = 100$.

Let λ_1 denote the largest absolute eigenvalue. On line-like structures, λ_1 has a large output. Since we are interested in dark elongated structures on a brighter background, only positive values of λ_1 are considered; pixels with negative values of λ_1 are set to zero. The feature image is subsequently constructed by inverting this image since the optimization is based on a minimum cost approach (see Fig. 2).

Next to the eigenvalues, the eigenvectors define the orientation of the line structure. The eigenvector corresponding to λ_2 is given by

$$\hat{e}_2 = \frac{(-I_{xy}/(I_{xx} - \lambda_2), 1)}{||(-I_{xy}/(I_{xx} - \lambda_2), 1)||}. \tag{19}$$

In the optimization scheme, we also investigated the use of the directional information to effectively attract the guide wire only to line structures with similar orientation. Hereto, the inner product between the spline and orientation of the feature is given by

$$O(\hat{x}_i) = \lambda_1(\hat{e}_2 \cdot \hat{x}_i) \tag{20}$$

where $\hat{x}_i$ is the normalized first derivative of the spline at sample point i. This means that, in the energy minimization (8), the external energy $F(i)$ is replaced by $O(i)$.

To be sensitive to guide wires of different width and to reduce sensitivity to noise, the feature image can be calculated at multiple scales (σ). This can also be used to enable a coarse-to-fine optimization strategy. A first estimate of the position of the spline can then be accomplished on a coarse scale. A coarse scale is less sensitive to local minima, and large displacements can be recovered. Subsequently, a more accurate localization can be determined using a smaller scale.

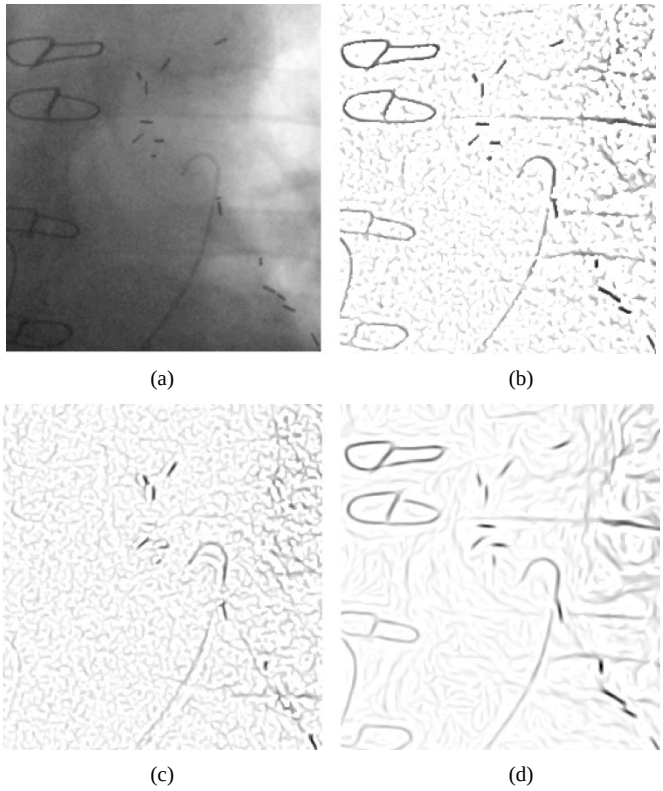

Fig. 2. (a) Fluoroscopic image of a guide wire in the thorax. (b) The feature image computed with the eigenvalues of the Hessian matrix with $\sigma = 1.5$ on the original image, (c) the subtracted image, and (d) the image preprocessed with CED. On the left-hand-side part of the image, stitches around the sternum are visible.

D. Acquisition

The method was applied on ten patient image sequences, with a sequence length between 14–50 frames, with a total of 267 frames. The dimension of the images is 512×512 and the approximate resolution is 0.4×0.4 mm^2 per pixel. The image series were acquired on an H5000, H3000, and a BV5000 X-ray fluoroscopy system (Philips Medical Systems, Best, The Netherlands) during clinical interventions. Only J-tipped guide wires were used during the interventions.

III. Evaluation

To evaluate the automatic method, a reference standard is constructed for every dataset. Therefore, three observers have manually outlined the guide wire in every image. They were able to see the whole movie to aid in drawing the guide wire in a single image. They also were instructed to draw a large part of the guide wire to ensure that a sufficiently large corresponding part to the automatically detected spline can be found.

This process was repeated after two weeks to limit the dependence between tracings. These six manually obtained paths are averaged to determine the average observer path $\bar{C}$ ("reference standard"), to which all individual paths will be compared. The intraobserver variability is then defined as

$$\text{Intra} = \sum_{k=1}^{K}\sum_{l=1}^{L}\sum_{m=1}^{M}\sum_{n=1}^{N}\frac{D(C_{klmn}, \bar{C}_{klm})}{KLMN} \tag{21}$$

where $D(C_1, C_2)$ denotes the distance between two curves, K is the number of image sequences $(K = 10)$, L is the number of frames in one sequence (L varies from 14 to 50), M represents the observer $(M = 3)$, and N denotes the number of the tracing $(N = 2)$. The interobserver variability is defined as the distance between individual tracings of observers and the reference standard

$$\text{Inter} = \sum_{k=1}^{K}\sum_{l=1}^{L}\sum_{m=1}^{M}\sum_{n=1}^{N}\frac{D(C_{klmn}, \bar{C}_{kl})}{KLMN}. \tag{22}$$

Likewise, to determine the accuracy of the automated method, the distance between the determined spline and the reference standard is defined as

$$\text{Error} = \sum_{k=1}^{K}\sum_{l=1}^{L}\frac{D(A_{kl}, \bar{C}_{kl})}{KL}. \tag{23}$$

For determining these numbers, a method to construct the average path $\bar{C}$ and a definition of the distance $D(C_1, C_2)$ between paths is required. To obtain the average path, first the corresponding parts of the paths are determined by finding the closest points of spline $C_1(C_2)$ to the endpoints of spline $C_2(C_1)$. The splines are then very densely resampled in an equal number of sample points (in this case, 1000), and $\bar{C}(i)$ is defined as the average of $C_1(i)$ and $C_2(i)$.

The distance metric $D(C_1, C_2)$ is defined as follows. First, we determine the minimum distance of a point $C_1(i)$ on the curve C_1 to a curve C_2 as

$$d_{\min}(C_1(i), C_2) = \min d(C_1(i), C_2(j)), \qquad j \in [1, N] \tag{24}$$

i.e., we search for the point on C_2 closest to $C_1(i)$. The mean distance between the curves C_1 and C_2 is now defined as

$$D(C_1, C_2) = \frac{1}{2N}\left(\sum_{i=1}^{N} d_{\min}\big(C_1(i), C_2\big) + \sum_{i=1}^{N} d_{\min}\big(C_1, C_2(i)\big)\right) \tag{25}$$

where N is chosen sufficiently large (1000) to limit discretization effects. Furthermore, both the distance from points on C_1 to C_2 and vice versa are determined in order to have a symmetric distance measure (i.e., $D(C_1, C_2) = D(C_2, C_1)$). The second measure that is calculated is the distance between the endpoints of the spline.

Input data for the method are as follows:

1) original image;
2) subtracted image;
3) image preprocessed with CED.

From these input data, feature images are constructed using the following:

1) image intensity;
2) Hessian filter at three scales;

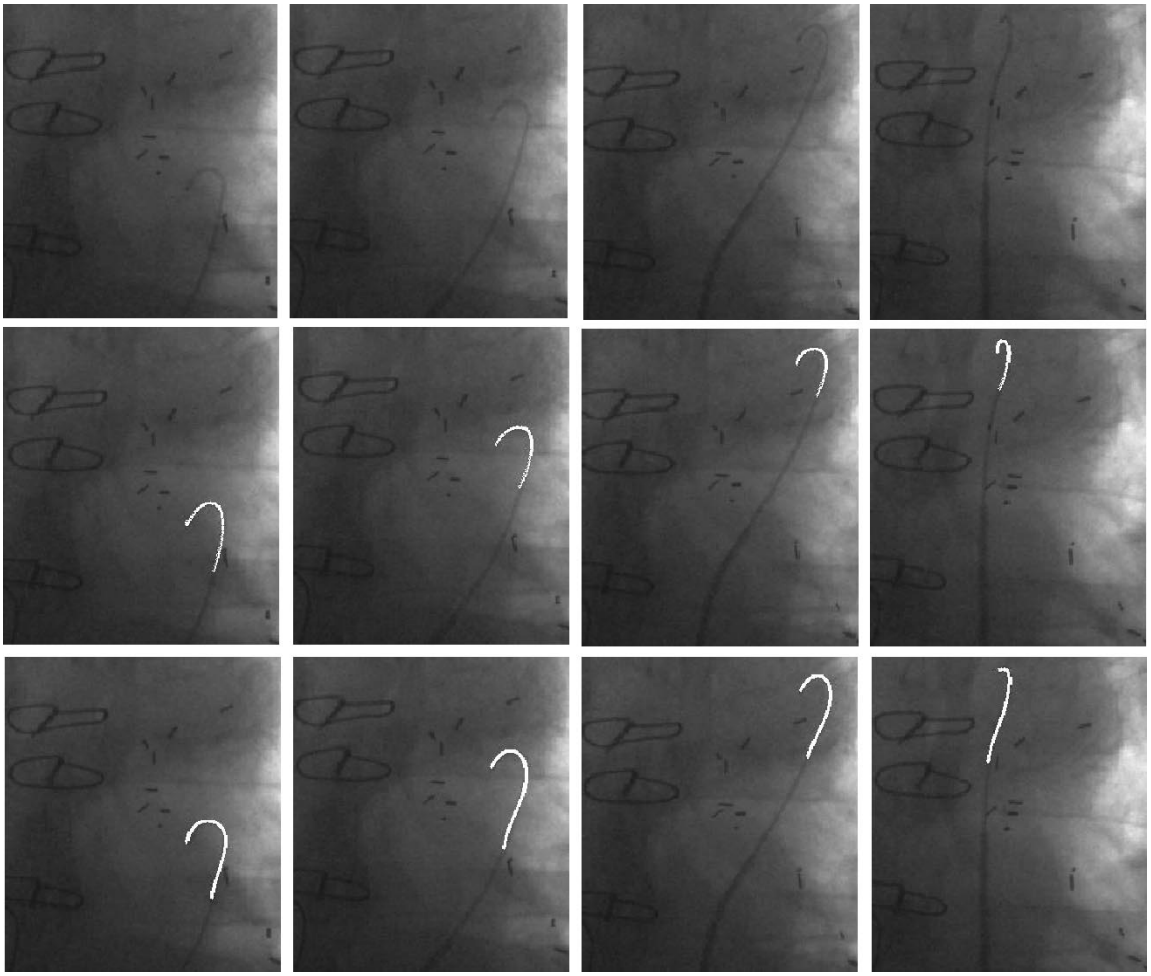

Fig. 3. Four frames (frames 2, 7, 16, and 27) out of a sequence of 30 frames, which gives an impression of the tracking results. The upper row is the original images of the sequence. The middle row is the resulting images when the method was applied on the feature image in which the eigenvalues of the Hessian matrix were calculated with $\sigma = 1.5$. The lower row is the reference standard obtained by manual tracings.

3) Hessian filter at three scales including orientation information

which yields a total of 21 combinations.

IV. Results

In this section, the results of the method are compared with the intraobserver and interobserver variability. An example of the tracking results is shown in Fig. 3. Here, a comparison with the results obtained by manual tracking is also visualized. All parameters in the experiments were kept fixed for all image sequences. CED was applied with $C = 1, \alpha = 0.001, \sigma = 1.0$ and the evolution was stopped at $t = 20$. The outliers and, thus, the tracking success, are based on visual inspection of the results. An outlier can clearly be identified since, in this case, the entire guide wire is misplaced (see Fig. 4). The mean and tip distances determined in the evaluation are only calculated for the successful tracking cases.

Table I summarizes the tracking results using the automatic method and shows the intraobserver and interobserver differences. The mean distance is the average distance between the corresponding parts of the splines, as described in Section III in pixel units. The mean tip distance is the distance between the endpoint of the reference standard and the endpoint of the automatic determined spline in pixel units. Between the brackets, the maximum distance is represented.

It was first checked whether only based on intensity, i.e., without enhancing line-like structures, the spline could successfully be tracked in the original image, subtracted image, and image preprocessed with CED. From Table I, it can be observed that the mean error of the automatic method for the original image and the image preprocessed with CED (1.05 pixels) does not differ significantly from the interobserver variability (1.04 pixels). However, the guide wire could only be tracked in 47% and 51%, respectively, of the frames due to the presence of other objects in the neighborhood of the guide wire in the image. Some improvement in tracking success was obtained using subtraction images. The guide wire could be tracked in 73% of the frames. Static line-like objects are not visible in the subtraction images, which gives an improvement of the tracking results. However, by performing digital subtraction, the noise level of the images is amplified, which makes the tracking more difficult.

It can be concluded that the intensity images are too noisy and, to increase the tracking success, a feature image is required.

Using the filter to enhance line-like structures, the tracking success rate greatly improves, while maintaining the same

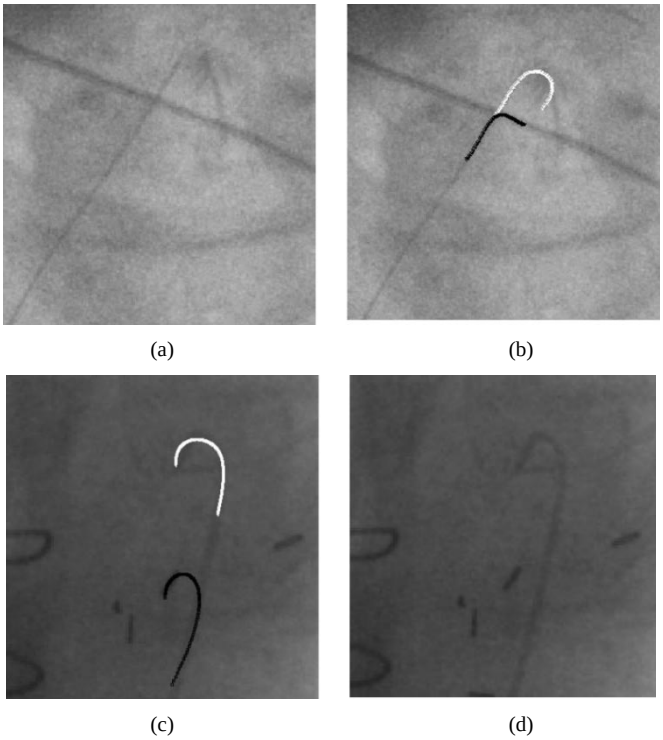

Fig. 4. Two examples of misplacement of the spline. (a) The original image. (b) The guide wire can be detected using the subtraction images (white spline), but using the Hessian image, the method failed (black spline). (c) An example where the guide wire was correctly detected using the Hessian with $\sigma = 1.5$ (white), but the method failed using $\sigma = 3.0$ (black). The spline is then more attracted to a stitch. (d) The original image in this case.

tracking accuracy. When applying the Hessian filter on the original images ("Original image"; see Table I) without direction information, best results are obtained at a scale $\sigma = 1.5$ pixel units. With these settings, the mean error of the automatic method (1.00 pixels) is approximately the same as the interobserver variability (1.04 pixels).

Owing to motion blur, the guide wire can sometimes become invisible in a number of sequences, which causes the spline to be incorrectly placed. Since motion blur mostly occurs in a single frame, it can be dealt with owing to a search region that is large enough for correct detection in the next frame. At a scale $\sigma = 1.5$ pixel units, the number of outliers in our evaluation was 11 frames (out of 267 frames) occurring in four sequences (out of ten sequences). These failures appeared mostly in a single frame. Without manual intervention, the guide wire was tracked correctly in the subsequent frames. In one sequence, the guide wire was lost in the last three frames owing to a line-like structure in the neighborhood of the guide wire.

For the tip distance, we can observe that the intraobserver and interobserver variability (1.09 and 1.46 pixels, respectively) is smaller than the error by the automatic tracking method (4.75 pixels) for $\sigma = 1.5$. Since the pixel size is approximately 0.4 mm, the mean error is approximately 2 mm.

If other scales ($\sigma = 1.0$ and $\sigma = 3.0$) are used during the eigenvalue computation, the performance becomes worse. Not only do the total distance and tip distance increase, but also the total number of outliers becomes larger. For smaller σ, the tracking results decrease, especially in the matching step. More often (in six sequences), the failure in one frame could not be corrected in the next frame, which causes a total loss of the guide wire. At a larger scale ($\sigma = 3.0$), broader line-like structures are enhanced, which causes a loss of the guide wire without manual intervention in five image sequences.

In Fig. 4, an example is shown where the guide wire could correctly be tracked using $\sigma = 1.5$ and where disturbing structures caused a mismatch using $\sigma = 3.0$.

If we use orientation information with scalar information in the optimization step, the results slightly improved at scales $\sigma = 1.5$ and $\sigma = 3.0$ pixel units. The number of outliers also decreased. Using orientation information, the spline is less attracted to enhanced structures with an orientation different from the spline. The optimization improves the localization of the spline, which subsequently influences the registration step in the next frame. At the optimal scale ($\sigma = 1.5$), the guide wire could be tracked correctly in 96% of the frames with subpixel accuracy (0.92 pixels). Comparing these results to the interobserver variability by using a T-test, no significant difference could be found, which implies that the automatic method has a similar accuracy as the observers.

We can observe that the performance of the method decreases when subtraction ("Subtracted Image"; see Table I) is used as a preprocessing step. Not only the mean distance increases, but also the total number of outliers becomes much larger. At scale $\sigma = 1.5$, the guide wire could only be tracked in 72% of the frames. Since the subtraction images are very noisy, not only line-like structures, but also noise, is enhanced. This causes a worsening of the tracking results. Adding orientation information in the optimization step could not improve the results. In fact, the total number of outliers increased, which resulted in a correct tracking in only 68% of the frames. An example where the Hessian feature image failed, but using subtraction as preprocessing step, the guide wire could correctly be detected is shown in Fig. 4.

When using the CED method as a preprocessing step ("CED image"; see Table I) prior to enhancing line-like structures, we can observe that the distance between the automatically determined spline and the reference standard is approximately the same as the interobserver variability for scales $\sigma = 1.5$ and $\sigma = 3.0$. The number of total outliers for this method was 38 frames out of 267 frames for $\sigma = 1.5$. However, in one sequence, a failure in 22 frames appeared, since the movement of the guide wire was too large, to correct for a single failure. Manual intervention at this point corrects this mismatch, which gives an actual number of outliers of 16, which implies a successful tracking in 94% of the frames. The other failures appeared only in a single frame, e.g., due to motion blur in the image sequence. Contrary to the results obtained on the original image sequence, results did not degrade significantly when altering the scale in the step of enhancing the guide wire. The mean tip distance was larger than interobserver variability for all scales, but did not exceed 2.5 mm.

If directional information is added in the external energy force, the results slightly improved for all different scales. The number of outliers decreased to 28 frames out of 267 frames for $\sigma = 1.5$. Again, in one sequence, a failure in a large number of

TABLE I

RESULTS FOR THE 21 COMBINATIONS OF THE METHOD COMPARED TO THE INTRAOBSERVERVARIABILITY AND INTEROBSERVERVARIABILITY (UPPER TWO ROWS). THE RESULTS ON THE ORIGINAL IMAGE, THE SUBTRACTED IMAGE, AND THE IMAGE PREPROCESSED WITH CED ARE LISTED IN THE THREE LOWEST ROWS. FROM THESE IMAGES, SEVEN FEATURE IMAGES HAVE BEEN CONSTRUCTED. BOTH THE ACCURACY AND TRACKING SUCCESS RATE HAVE BEEN LISTED. IT CAN BE OBSERVED THAT THE USE OF TECHNIQUES TO ENHANCE LINE-LIKE STRUCTURES GREATLY IMPROVE THE TRACKING SUCCESS WHILE MAINTAINING THE SAME TRACKING ACCURACY. ()* = TRACKING SUCCESS AFTER MANUAL INTERVENTION IN ONE FRAME

	Image feature	Scale (pixels)	Mean (max) distance (pixels)	Mean (max) tip distance (pixels)	Tracking success (%)
Intra observer			0.66 [1.46]	1.09 [1.77]	100%
Inter observer			1.04 [2.19]	1.46 [2.44]	100%
Original image	Intensity	-	1.05 [1.64]	3.75 [7.07]	47%
	Hessian without orientation	$\sigma = 1.0$	1.18 [1.56]	5.99 [9.65]	70%
		$\sigma = 1.5$	1.00 [1.58]	4.75 [10.60]	95%
		$\sigma = 3.0$	1.08 [1.55]	5.93 [10.85]	84%
	Hessian with orientation	$\sigma = 1.0$	1.26 [3.10]	5.81 [9.35]	76%
		$\sigma = 1.5$	**0.92 [1.49]**	**4.38 [8.20]**	**96%**
		$\sigma = 3.0$	1.05 [1.47]	5.70 [10.92]	88%
Subtracted image	Intensity	-	1.29 [2.05]	5.38 [13.18]	73%
	Hessian without orientation	$\sigma = 1.0$	1.30 [1.97]	5.40 [11.08]	66%
		$\sigma = 1.5$	1.15 [1.73]	5.10 [11.42]	72%
		$\sigma = 3.0$	1.44 [2.85]	6.04 [9.83]	76%
	Hessian with orientation	$\sigma = 1.0$	1.27 [2.05]	4.92 [10.22]	54%
		$\sigma = 1.5$	1.25 [2.06]	5.51 [9.02]	68%
		$\sigma = 3.0$	1.27 [1.94]	5.48 [10.97]	62%
CED image	Intensity	-	1.05 [2.31]	3.94 [8.85]	51%
	Hessian without orientation	$\sigma = 1.0$	1.13 [2.18]	4.42 [9.07]	84%
		$\sigma = 1.5$	0.99 [1.97]	5.31 [11.16]	86% (94%)*
		$\sigma = 3.0$	0.99 [1.36]	5.43 [8.94]	88%
	Hessian with orientation	$\sigma = 1.0$	1.04 [1.74]	4.95 [12.50]	87%
		$\sigma = 1.5$	**0.96 [1.67]**	**4.33 [6.18]**	**90% (96%)***
		$\sigma = 3.0$	0.92 [1.50]	5.33 [11.98]	91%

frames appeared (18 frames), which could be corrected for with manual intervention. This gives an actual number of outliers of ten and a correct tracking in 96% of the frames.

V. DISCUSSION AND CONCLUSION

A method has been developed to automatically track the guide wire in fluoroscopic guided interventions. During these interventions, 12.5 frames/s are acquired, thus, manual outlining is not an option. The method is based on a spline optimization in an image where line-like structures are enhanced with or without the use of orientation information. As a preprocessing step, the use of subtraction and CED is investigated. In order to assess whether the proposed method is sufficiently accurate, tracings of observers were acquired in 267 frames. Due to presence of guide-wire-like objects in the neighborhood of the guide wire and a low SNR, tracking is not successful using intensity images. Using the Hessian feature image calculated on both the original image and the image preprocessed with CED, the accuracy of spline localization was similar to the interobserver variability. Using orientation information, the results slightly improved. Subtraction as a preprocessing step degraded the results due to the amplification of the noise level in the images. Adding orientation information could not improve the results in this case. The scale at which the method performed best was $\sigma = 1.5$ pixels in our case. This parameter can also be optimized by inspecting the grey-value profile perpendicular to the spline.

The method detected the guide wire correctly in 96% of the frames when orientation information was used in the optimization step. With the optimal settings, outliers occurred mainly in

one single frame owing to motion blur. Given the high temporal resolution (12.5 frames/s) missing one frame does not hamper the interventional radiologist. In fact, in most of these frames, the guide wire is not visible to the radiologist either. The tip of the guide wire could be localized within an accuracy of approximately 2 mm, which is less accurate than the manual observers. Depending on the required accuracy, the method could be extended with an explicit endpoint localization. Whereas the use of CED did not significantly improve the accuracy if the proper scale was used for enhancing line-like structures, the results were more robust with respect to changing the scale parameter. This indicates that the use of CED is useful for robustness in clinical practice.

The algorithm currently takes approximately 5 s per frame. By optimizing the code and using a faster PC and/or by using hardware solutions, the acquired speed-up factor for real time use (approximately 60 times) can be achieved without compromising the robustness and accuracy of the algorithm.

REFERENCES

[1] D. Palti-Wasserman, A. M. Brukstein, and R. P. Beyar, "Identifying and tracking a guide wire in the coronary arteries during angioplasty from X-ray images," *IEEE Trans. Biomed. Eng.*, vol. 44, pp. 152–164, Feb. 1997.

[2] H. Starkhammar, M. Bengtsson, and D. A. Kay, "Cath-finder catheter tracking system: A new device for positioning of central venous catheters. Early experiments from implantation of brachial portal systems," *Acta. Anaesthesiol. Scand.*, no. 34, pp. 296–300, 1990.

[3] J. Ragasa, N. Shan, and R. W. Watson, "Where antecubital catheters go: A study under fluoroscopic control," *Anesthesiology*, no. 71, pp. 378–380, 1989.

[4] H.-J. Bender, R. Männer, C. Poliwoda, S. Roth, and M. Walz, "Reconstruction of 3D catheter paths from 2D X-ray projections," in *Medical Image Computing and Computer-Assisted Intervention*, ser. Lecture Notes in Computer Science. Berlin, Germany: Springer-Verlag, 1999, vol. 1679, pp. 981–989.

[5] S. Aylward, E. Bullit, S. Pizer, and D. Eberly, "Intensity ridge and widths for tubular object segmentation and description," *Math. Meth. Biomed. Image Anal.*, pp. 131–138, 1996.

[6] Y. P. Du, D. L. Parker, and W. L. Davis, "Vessel enhancement filtering in three-dimensional MR angiography," *J. Magn. Reson. Imag.*, vol. 5, no. 3, pp. 353–359, 1995.

[7] K. R. Hoffmann *et al*., "A system for determination of 3D vessel tree centerlines from biplane images," *Int. J. Cardiac Imag.*, vol. 16, no. 5, pp. 315–330, 2000.

[8] A. K. Klein, F. Lee, and A. A. Amini, "Quantitative coronary angiography with deformable spline models," *IEEE Trans. Med. Imag.*, vol. 16, pp. 468–482, May 1997.

[9] T. Koller, G. Gerig, G. Székely, and D. Dettwiller, "Multiscale detection of curvilinear structures in 2-D and 3-D image data," in *Eur. Conf. Computer Vision*, 1995, pp. 864–869.

[10] R. Kutka and S. Stier, "Extraction of line properties based on direction fields," *IEEE Trans. Med. Imag.*, vol. 15, pp. 51–58, Jan. 1996.

[11] C. Lorenz, I.-C. Carlsen, T. M. Buzug, C. Fassnacht, and J. Weese, "Multi-scale line segmentation with automatic estimation of width, contrast, and tangential direction in 2D and 3D medical images," in *Computer Vision, Virtual Reality and Robotics in Medicine–Medical Robotics and Computer Assisted Surgery*, ser. Lecture Notes in Comput. Sci. Berlin, Germany: Springer-Verlag, vol. 1205, pp. 233–242.

[12] R. Poli and G. Valli, "An algorithm for real-time vessel enhancement and detection," *Comput. Meth. and Programs Biomed.*, vol. 52, pp. 1–22, 1997.

[13] Y. Sato, S. Nakajima, H. Atsumi, S. Yoshida, T. Koller, G. Gerig, and R. Kikinis, "Three-dimensional multi-scale line filter for segmentation and visualization of curvilinear structures in medical images," *Med. Image Anal.*, vol. 2, no. 2, pp. 143–168, 1998.

[14] D. L. Wilson and J. A. Noble, "Segmentation of cerebral vessels and aneurysms, from MRA data," in *Information Processing in Medical Imaging*, ser. Lecture Notes in Comput. Sci. Berlin, Germany: Springer-Verlag, 1997, pp. 423–428.

[15] M. Fischler, J. Tenenbaum, and H. Wolf, "Detection of roads and linear structures in low-resolution aerial imagery using a multisource knowledge integration," *Comput. Graph. Image Process.*, vol. 15, pp. 201–223, 1981.

[16] C. Steger, "An unbiased detector of curvilinear structures," *IEEE Trans. Pattern Anal. Machine Intell.*, vol. 20, pp. 113–125, Feb. 1998.

[17] A. L. Yuille, P. W. Hallinan, and D. S. Cohen, "Feature extraction from faces using deformable templates," *Int. J. Comput. Vis.*, vol. 8, no. 2, pp. 99–111, 1992.

[18] M. La Cascia, S. Sclaroff, and V. Athitsos, "Fast, reliable head tracking under varying illumination: An approach based on registration of texture-mapped 3D models," *IEEE Trans. Pattern Anal. Machine Intell.*, vol. 22, pp. 322–336, Apr. 2000.

[19] N. Paragios and R. Deriche, "Geodesic active contours and level sets for the detection and tracking of moving objects," *IEEE Trans. Pattern Anal. Mach. Intell.*, vol. 22, pp. 266–280, Mar. 2000.

[20] W. H. Press, S. A. Teukolsky, W. T. Vetterling, and B. P. Flannery, *Numerical Recipes in C: The Art of Scientific Computing*. Cambridge, U.K.: Cambridge Univ. Press, 1992.

[21] E. H. W. Meijering, W. J. Niessen, and M. A. Viergever, "Retrospective motion correction in digital subtraction angiography: A review," *IEEE Trans. Med. Imag.*, vol. 18, pp. 2–21, Jan. 1999.

[22] J. Weickert, "Coherence-enhancing diffusion filtering," *Int. J. Comput. Vis.*, vol. 31, no. 2/3, pp. 111–127, 1999.

[23] M. Kass, A. Witkin, and D. Terzopoulos, "Snakes: Active contour models," *Int. J. Comput. Vis.*, vol. 1, no. 4, pp. 321–331, 1987.